Nanoscale

Accepted Manuscript

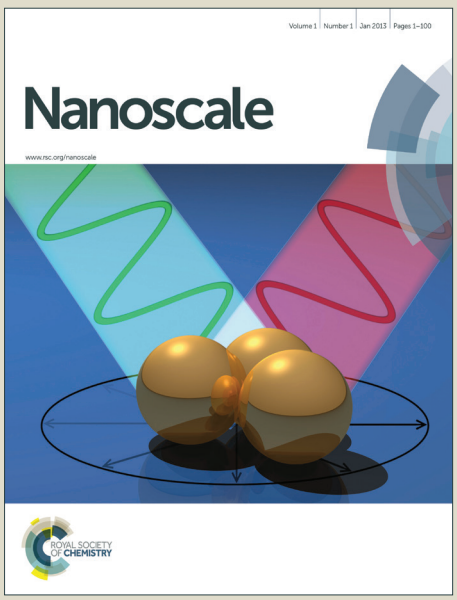

ROYAL SOCIETY OF CHEMISTRY

www.rsc.org/nanoscale

Epidermal growth factor receptor-targeted lipid nanoparticles retain self-assembled nanostructures and provide high specificity

Jiali Zhai[1*], Judith A. Scoble[2], Nan Li[1, 3], George Lovrecz[1], Lynne J. Waddington[2], Nhiem Tran[1], Benjamin W. Muir[1], Gregory Coia[2], Nigel Kirby[5], Calum J. Drummond[4], Xavier Mulet[1*]

[1] CSIRO Manufacturing Flagship, Private Bag 10, Clayton, VIC 3169, Australia

[2]CSIRO Manufacturing Flagship, 343 Royal Parade, Parkville, VIC 3052, Australia

[3]Department of Respiratory Medicine, Shanghai Pulmonary Hospital, Tongji University School of Medicine, Shanghai 200433, China

[4]School of Applied Sciences, College of Science Engineering and Health, RMIT University, GPO Box 2476, Melbourne, Vic 3001, Australia

[5]Australian Synchrotron, 800 Blackburn Rd, Clayton, Vic 3168, Australia

*Corresponding authors: xavier.mulet@csiro.au; maggie.zhai@csiro.au

Abstract

Next generation drug delivery utilising nanoparticles incorporates active targeting to specific sites. In this work, we combined targeting with the inherent advantages of self-assembled lipid nanoparticles containing internal nanostructures. Epidermal growth factor receptor (EGFR)-targeting, PEGylated lipid nanoparticles using phytantriol and 1,2-distearoyl-sn-glycero-3-phosphoethanolamine-PEG-maleimide amphiphiles were created. The self-assembled lipid nanoparticles presented here have internal lyotropic liquid crystalline nanostructures, verified by synchrotron small angle X-ray scattering and cryo-transmission electron microscopy, that offer the potential of high drug loading and enhanced cell penetration. Anti-EGFR Fab' fragments were conjugated to the surface of nanoparticles via a maleimide-thiol reaction at a high conjugation efficiency and retained specificity following conjugation to the nanoparticles. The conjugated nanoparticles were demonstrated to have high affinity for an EGFR target in a ligand binding assay.

Keywords: EGFR, bioconjugation, lyotropic liquid crystalline, lipid nanoparticles, cubosomes, hexosomes, liposomes, synchrotron SAXS, targeted drug delivery.

Introduction

One of the ultimate aims in the development of anti-cancer nanomedicines is to confine the treatment to the target tumour and reduce off-target side effects. This can be achieved through actively targeting chemotherapeutic drugs. Therapeutically loaded nanoparticle-based systems have been extensively explored in the field of targeted drug delivery due in part to their ability to deliver high payloads.[1-4] Taking advantage of the anatomic and pathophysiological properties of the tumour, nanoparticle-based drug delivery systems offer innate passive targeting characteristics through the enhanced permeation and retention (EPR) effect.[5, 6]

Active targeting involves conjugating a targeting moiety that can facilitate nanoparticle binding to the tumour cells and/or cellular internalisation.[7, 8] Monoclonal antibodies (mAb) and their antigen binding fragments (Fab') are common targeting moieties that specifically recognise cell surface receptors. For example, the epidermal growth factor receptor (EGFR) family is one of the most studied receptors. It is over-expressed on a number of cancer cells than in normal healthy cells, mediating cancer cell proliferation, metastasis, and angiogenesis.[9, 10] Therefore, EGFR mAbs have been developed with EGFR targeting activity and anti-tumour efficacy.[11-13] Studies have shown enhanced efficacy of mAb- or Fab'-conjugated nanoparticles when compared to 'bare' nanoparticles, attributable to active targeting of the tumours.[14-17]

In lipid nanoparticle drug delivery systems, mAb- or Fab'-functionalised liposomes have been extensively exploited to achieve active targeting.[18-20] Liposomes functionalised with mAb or Fab' targeting EGFR,[20, 21] human epidermal growth factor receptor 2 (HER2),[22, 23] and epithelial cell adhesion molecule (EpCAM)[24] have previously been developed. A common strategy to link targeting moieties to the liposome surface is via a poly(ethylene

glycol) (PEG) spacer.[18, 25, 26] Specifically, one end of the PEG has a chemical handle such as a maleimide or a biotin group for bioconjugation to targeting moieties; the other end is composed of a lipidic anchor to attach the functionalised PEG to the surface of the lipid nanoparticle. The PEG corona around the nanoparticle is essential for reducing non-specific opsonin binding, resulting in less immunogenicity and enhanced circulation times *in vivo.*[27-29] Studies have shown that EGFR-targeting, PEGylated liposomes prepared using 1,2-distearoyl-sn-glycero-3-phosphoethanolamine-PEG-maleimide (DSPE-PEG-mal) and anti-EGFR Fab' at the particle surface had improved cellular uptake and anti-tumour efficacy.[20, 21]

Lipid-based lyotropic liquid crystalline nanoparticles (LCNPs), such as cubosomes and hexosomes, stabilised by PEG-based polymers, are emerging as promising self-assembled lipid nanoparticles for drug delivery (Figure 1).[30-46] As described in a number of recent reviews,[37, 47] cubosomes and hexosomes are lipid dispersions of the inverse bicontinuous cubic phase and the inverse hexagonal phase, respectively, with a typical particle size distribution of 100-250 nm. Cubosomes and hexosomes possess high surface area and extensive meso porosity.[37, 47] Studies have shown that advantages of these nano-structured LCNPs over other drug delivery systems include high encapsulation efficiency of both hydrophobic and amphiphilic drugs whilst their inherent meso porosity provides a mechanism for controlled release.[36, 38, 44] Yet, to date there are limited studies on surface-functionalisation of these LCNP nanoparticles for active targeting of the encapsulated therapeutics and for protein entrapment and loading.[48-53]

A few studies used lipid-PEG polymers such as maleimide(triethylene glycol)ether lipid,[49] DSPE-$PEG_{Mw=2000}$-biotin[51] and oleate-PEG-maleimide[53] in an attempt to make surface-functionalised LCNPs, but the main stabiliser in the formulation was still Pluronic F127, a polydisperse PEO_{100}-PPO_{65}-PEO_{100} triblock copolymer. Although Pluronic F127 is the most commonly used polymer in making LCNPs,[54, 55] it does not contain functional

groups for bioconjugation. It is interesting to investigate the ability of DSPE-PEG polymers to substitute Pluronic F127 for the purpose of stabilisation, and most importantly, surface-functionalisation for bioconjugation.

We have constructed stable phytantriol-based LCNPs with internal nano-structure for drug loading and surface functionalisation for bioconjugation using DSPE-PEG-mal. Actively targeted LCNPs were prepared from phytantriol cubosomes and hexosomes with anti-EGFR Fab' conjugated to the nanoparticle surface via the maleimide-thiol reaction (Figure 1). Synchrotron small angle X-ray scattering (SAXS) and cryo-transmission electron microscopy (cryo-TEM) were used to confirm the presence of the lyotropic liquid crystalline phases. The conjugation efficiency of anti-EGFR Fab' to LCNPs was compared in parallel to liposomes also functionalised by DSPE-PEG-mal. Finally, the EGFR binding activity of the conjugated anti-EGFR Fab' on LCNPs was confirmed by a ligand binding assay.

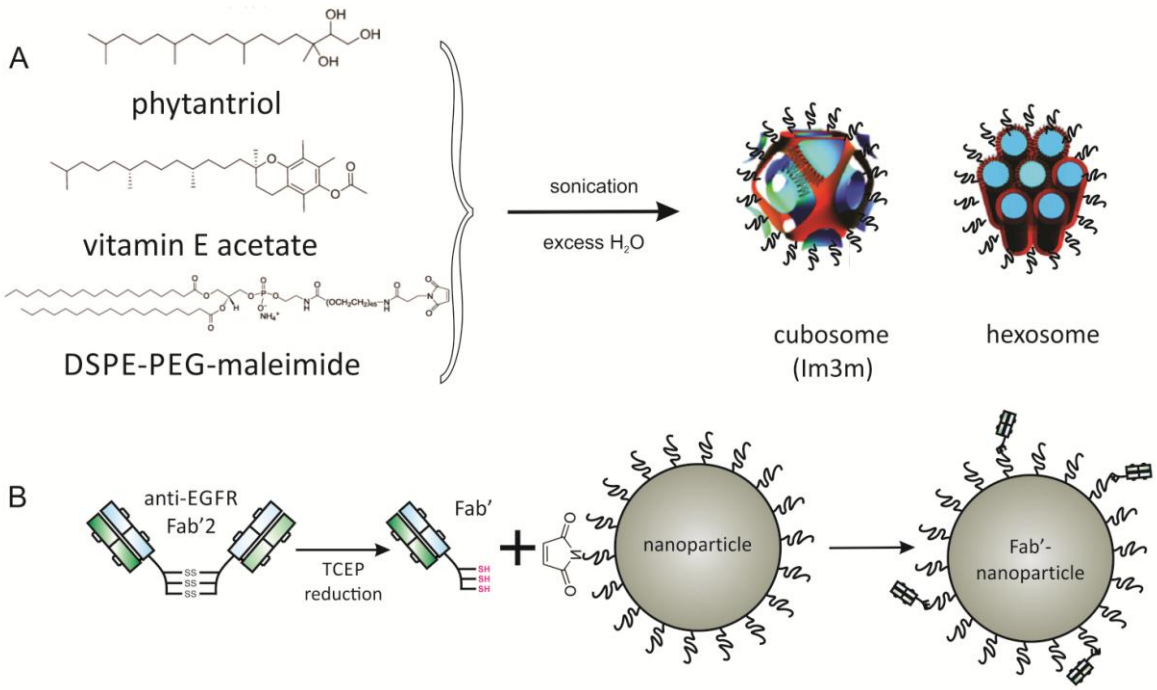

Figure 1: A) Molecular structures of the amphiphiles and the fabrication of LCNPs with their internal nano-structures by sonication in excess water. B) Partial reduction of anti-EGFR Fab'2 to yield the Fab' fragment with three active thiol groups (-SH) in the hinge region that react with the maleimide group on the nanoparticle surface.

Experimental

1. *Materials*

1,2-Distearoyl-sn-glycero-3-phosphocholine (DSPC) was purchased from Avanti Polar Lipids, Inc. 1,2-distearoyl-sn-glycero-3-phosphoethanolamine-$PEG_{Mw=3400}$-maleimide (DSPE-$PEG_{Mw=3400}$-mal) was purchased from Nanocs Inc. Phytantriol was a gift from DSM. Phosphate buffered saline (PBS, pH 7.4), cholesterol, vitamin E acetate, iodoacetamide, tris(2-carboxyethyl)phosphine hydrochloride (TCEP), protein G and albumin from chicken egg white were purchased from Sigma-Aldrich. DELFIA Enhancement Solution was purchased from Perkin Elmer. All other chemicals and solvents were of analytical grade. Milli-Q H_2O (18.2 MΩ) was used for all aqueous preparations. All compounds were used without further purification.

2. *Preparation of lipid nanoparticles*

LCNPs, i.e. cubosomes and hexosomes, were prepared using phytantriol, a common amphiphilic lipid used in the formation of LCNPs.[56-58] For cubosome preparation, DSPE-$PEG_{Mw=3400}$-mal (1 mM) serving as both the stabiliser and the functional molecule for surface bioconjugation was added to phytantriol (70 mM) (Table 1). For hexosome preparation, the third ingredient, vitamin E acetate (4 mM), was added to induce a phase transition to the hexagonal phase from the cubic phase.[57] PBS was then added to the lipid phase and the mixture was sonicated by a probe sonicator (Heat systems-Ultrasonics, Inc.) with a 5 s-on, 5 s-off mode for a total of 2 min.

PEGylated liposomes were prepared by thin lipid film formation followed by hydration and extrusion through polycarbonate membranes. DSPC (20 mM), cholesterol (10 mM) and DSPE-$PEG_{Mw=3400}$-mal (1 mM) were dissolved in a chloroform and methanol mixture (Table 1). A thin lipid film was prepared using N_2 gas and placed under vacuum overnight. The PBS-hydrated lipid film was sonicated in a water bath sonicator (Unisonics) at

60 °C for 30 min. The sonicated solution was then extruded 11 times through a 0.1 µm polycarbonate membrane (Nuclepore Track-Etch Membrane, Whatman) using a mini-extruder (Avanti Polar Lipids, Inc.).

Table 1: Composition and particle size distribution of lipid nanoparticles.

		Cubosomes	hexosomes	Liposomes
Lipid composition (molar ratio)		Phyt:DSPE-PEG-mal (74:1)	Phyt:VitEA:DSPE-PEG-mal (74:4:1)	DSPC:Cholesterol:DSPE-PEG-mal (20:10:1)
Particle size (nm)	fresh	232±18	251±18	90±15
	2 months	227±26	255±23	88±15
	After conjugation	235±15	246±30	91±13
PDI	fresh	0.13±0.01	0.2±0.1	0.14±0.01
	2 months	0.1±0.1	0.2±0.1	0.15±0.12
	After conjugation	0.18±0.05	0.15±0.11	0.16±0.05

Abbreviations: Phyt (phytantriol); VitEA (vitamin E acetate); DSPE-PEG-mal (1,2-distearoyl-sn-glycero-3-phosphoethanolamine-$PEG_{Mw=3400}$-maleimide); PDI (polydispersity index).
Note: Particle size distribution was measured in triplicates of 3 individual samples. Measurement was performed following fresh preparation and after 2 month storage at 4 °C.

3. Conjugating anti-EGFR Fab' to lipid nanoparticles

The mouse hybridoma cell line (ATCC HB8509) secreting the 528 mAb was grown in the CSIRO Protein Production Facility in Parkville, and the 528 mAb purified by Protein A chromatography (GE Healthcare) before being cleaved with pepsin (1 mg pepsin to 200 mg mAb) in 0.1 M citrate buffer, pH 3.5, for 30 min at 37 °C to produce the Fab'2 fragment, which was isolated by gel filtration on a Superdex 200 26/60 column (GE Healthcare) equilibrated with PBS. Fab'2 fragments were partially reduced at a molar ratio of three TCEP per Fab'2 at room temperature for 2 hrs to yield a mixture of Fab'2 and Fab' fragments. The Fab' was isolated by gel filtration on a Superdex S200 10/30 column equilibrated with PBS containing 0.5 mM EDTA (pH 7.4). The concentration of free thiol groups was determined using Ellman's reagent as previously described.[59, 60] It was found that three thiol groups were present on each Fab'. To prevent reduced thiol groups from being re-oxidised, Fab' fragments were freshly prepared prior to the conjugation experiment.

Purified Fab' fragments and nanoparticles were incubated overnight at 4 °C for the conjugation reaction to occur. Optimisation of conjugation efficiency was achieved by varying the maleimide-to-thiol reaction ratio. Following overnight incubation, aliquots of iodoacetamide, to a final concentration of 17 mg/mL, was added to the conjugated samples to quench further reactions.

SDS-PAGE analysis on an XCell SureLock™ Mini-Cell Electrophoresis System (Invitrogen) was performed to confirm the conjugation of Fab' to nanoparticles. Conjugation efficiency in percentage was calculated by integrating the stained gels using ImageJ software.[61]

$$\text{Conjugation efficiency} = \frac{\text{amount of conjugated Fab}'}{\text{total amount of Fab}'} \times 100\%$$

4. Particle size distribution measurement

Particle size distribution of the nanoparticles was measured using a Malvern Zetasizer Nano ZS (Malvern Instruments, U.K.). Samples were diluted and transferred to disposable low-volume plastic cuvettes. Samples were analysed at 25 °C with refractive indices of phospholipids or phytantriol as materials and PBS as the bulk diluent to calculate the hydrodynamic particle sizes.

5. Synchrotron SAXS measurement

Synchrotron SAXS measurement was performed at the SAXS/wide-angle X-ray scattering (WAXS) beamline at the Australian Synchrotron. The X-ray had a beam with a wavelength of λ = 1.033 Å (11.0 keV) with a typical flux of approximately 10^{13} photons/s. 2D X-ray diffraction patterns were recorded on a Decris-Pilatus 1-M detector of 10 modules. A silver behenate standard (λ = 58.38 Å) was used for calibration. Samples were loaded in a 96-well, half-area UV clear plate (Greiner) and positioned in a custom-designed plate holder with the temperature controlled at 25 ± 0.1 °C via a recirculating water bath as previously

described.[62] The exposure time for each sample was 1 s. SAXS data were analysed using the IDL-based AXcess software package to examine the lyotropic liquid crystalline phase identity and the lattice parameter within the nanoparticles.[63]

6. Purification of Fab' conjugated nanoparticles

For conjugated liposomes, unbound Fab' was removed by gel filtration on a Superose 12 10/30 column (GE Healthcare) equilibrated with PBS buffer (pH 7.4) on an AKTA FPLC system (GE Healthcare). To avoid pressurised gel filtration system for better retainment of the internal liquid crystalline nanostructures of cubosomes and hexosomes, dialysis method was used to remove the trace amount of unbound Fab' in conjugated samples of cubosomes and hexosomes. Dialysis was conducted using 300 kDa MWCO Float-A-Lyzer devices (Spectra/Por) for 24 hours in PBS buffer (pH 7.4) with at least 3 times of buffer changes.

7. *Cryo-TEM*

Cryo-TEM was used to visualise the formulated nanoparticles. Copper grids (200-mesh) coated with perforated carbon film (Lacey carbon film, ProSci Tech, Australia) were glow discharged in nitrogen to render them hydrophilic and placed in a laboratory-built humidity-controlled vitrification system. Aliquots of samples were applied onto the grids and after 30 s adsorption time, grids were blotted manually by filter paper for approximately 3 s. Grids were then plunged into liquid ethane cooled by liquid nitrogen. Images were recorded using a Tecnai 12 transmission electron microscope (TEM) operating at 120 kV, equipped with an FEI Eagle 4k×4k CCD, (FEI, Eindhoven, The Netherlands). At all times low dose procedures were followed limiting the electron dose to no more than 10 electrons/$Å^2$.

8. Ligand binding assay

A solution form of the EGFR, sEGFR501.Fc,[64-66] and the europium-labelled epidermal growth factor (Eu-EGF, Perkin Elmer) were used to assess the binding activity of anti-EGFR Fab' of the 528 mAb and the corresponding nanoparticle conjugates.

sEGFR501.Fc is a truncated fragment of EGFR fused with the IgG Fc region. It has high affinity for various EGFR ligands and contains the epitope that is recognised by the 528 mAb used in this study. A competition assay was performed by monitoring the europium signal in a time-resolved fluorescence (TRF) mode. Briefly, 96-well Lumitrac plates (Greiner) were coated overnight at 4 °C with protein G at a concentration of 2 µg/mL in 10 mM sodium citrate buffer, pH 6.0, followed by blocking with 0.5% albumin in Tris buffered saline (TBS). After 3 washes with TBS containing 0.05% Tween 20 (TBST), sEGFR501.Fc at a concentration of 500 ng/mL in TBST was added to the plates and incubated overnight at 4 °C. A 100 pM solution of Eu-EGF in ligand binding buffer (100 mM HEPES, 100 mM NaCl, 2 µM diethylenetriaminepentaacetic acid, pH 7.6) was used as the diluent to prepare a series of dilutions of either free anti-EGFR Fab' or Fab'-conjugated nanoparticles. Diluted samples were added in triplicates to the plates and incubated for 1 hr at room temperature. After 3 washes with TBST, DELFIA Enhancement Solution was added to the plate followed by incubation for 20 min at room temperature. Quantification of TRF signals was performed on a Victor^2 1420 multilable plate reader (Perkin Elmer). Values are normalised as percentages of the signal of Eu-EGF alone (100 pM) and plotted against Log(M) Fab' whether the Fab' was free or conjugated. The inhibition curve was fitted by GraphPad Prism (GraphPad Software Inc.) using the competitive binding, non-linear regression analysis to calculate approximate IC50 values.

Results and Discussion

We created, characterised and quantified the active targeting of phytantriol-based LCNPs conjugated with anti-EGFR Fab' of the 528 mAb on the particle surface using the maleimide-thiol chemistry (Figure 1). DSPE-$PEG_{Mw=3400}$-mal polymers had a dual role of dispersion-stabilisation and surface-functionalisation in fabricating the phytantriol-based LCNPs (Figure 1). The particle sizes were 232 nm and 251 nm for cubosomes and hexosomes, respectively, and these formulations were stable for at least two months (Table 1). Anti-EGFR Fab'2 was partially reduced by TCEP yielding three thiol groups in the hinge region (Figure 1B). Bioconjugation was then achieved by incubation of the reactive Fab' and the maleimide-functionalised nanoparticles. The maleimide double bond underwent Michael addition with the thiol group, forming a stable thiol-ether bond to attach the Fab' to the nanoparticle surface (Figure 1B).

1. *Fabrication of functionalised LCNPs and their lipid self-assembled nano-structures*

We found that DSPE-$PEG_{MW=3400}$ polymer provided sufficient stabilisation to phytantriol-based LCNPs. It has an average PEG chain length of 70 and was used at the same phytantriol-to-polymer ratio in the formulation as Pluronic F127. At a molar ratio of 74 phytantriol lipid chains per DSPE-$PEG_{MW=3400}$ molecule, the polymer provided sufficient stabilisation effect to completely substitute Pluronic F127, achieving stabilisation and surface-functionalisation of phytantriol nanoparticles in cubosome or hexosome form. Confirmation of the internal structure of the LCNPs was performed using synchrotron SAXS. Phytantriol nanoparticles adopted a primitive inverse bicontinuous cubic phase (Im3m space group) with a lattice parameter of 98.7 Å (Figure 2A). The addition of vitamin E acetate to phytantriol induced a phase change to hexosomes with a lattice parameter of 50 Å (Figure 2B).

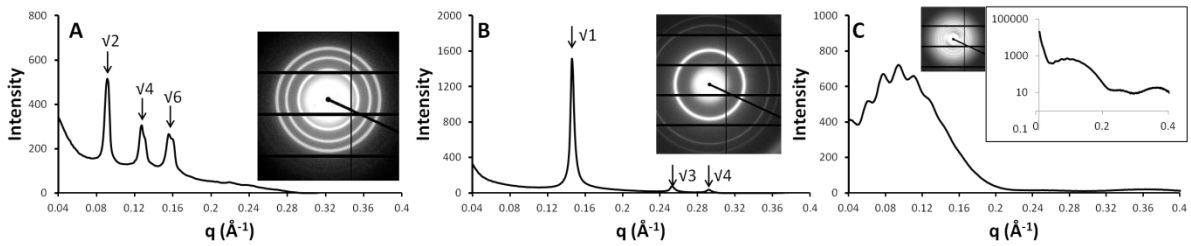

Figure 2: Synchrotron small angle X-ray (SAXS) 2D diffraction patterns and corresponding 2D SAXS profiles of A) phytantriol cubosomes, B) phytantriol hexosomes, and C) unilamellar liposomes. Insert in C) is a log scale plot of the liposome diffraction. All nanoparticles contained 1 mM DSPE-$PEG_{Mw=3400}$-mal as the functional ingredient. Detailed composition and the molar ratio are in Table 1.

Phytantriol is known to form the double diamond cubic phase (Pn3m space group) in excess water or when dispersed as nanoparticles stabilised by Pluronic F127.[55-58] The change to the primitive cubic phase (Im3m space group) observed here suggests that the hydrophobic DSPE lipidic group inserts within the non-polar phytantriol layer, reducing the interfacial curvature of the lipid monolayer and forming the primitive cubic phase (crystallographic space group Im3m) rather than the double diamond cubic phase (Pn3m space group). The hydrophilic PEG block extends from the surface of the nanoparticles offering steric stability thus preventing particle aggregation. A recent study by Nilsson et al. investigated the effect of incorporating DSPE-$PEG_{MW=2000}$ on the liquid crystalline phase of phytantriol cubosomes and also observed a transition from the double diamond cubic phase to the primitive cubic phase (space group Im3m).[67]

Unilamellar liposomes made of DSPC, cholesterol and DSPE-$PEG_{MW=3400}$-mal were prepared by the extrusion method and used for comparison with LCNPs in bioconjugation experiments. This composition of DSPC and cholesterol was chosen for comparison with immunoliposomes made in previous studies.[20, 21] The liposomes in this study had a particle size of approximately 90 nm (Table 1). The scattering pattern from liposomes in this study (Figure 2C inset) exhibits a broad lobe in the q range of 0.04 - 0.2 $Å^{-1}$. This is representative

of scattering of unilamellar vesicles and is consistent with previous studies using a synchrotron SAXS technique to examine diffraction of unilamellar liposomes.[68, 69] Overlaid on the liposomal scattering, small undulations in the q range of 0.04-0.12 $Å^{-1}$ can be observed (Figure 2C). Similar undulations have been reported in previous studies.[70, 71] These small peaks do not correspond to any other known lyotropic liquid crystalline phases such as the cubic or hexagonal phases. Further evidence that the extrusion method yielded unilamellar liposomes is evidenced in the liposome cryo-TEM images provided in Supplementary Figure S2. The morphology of the samples showed mostly unilamellar liposomes with a very small fraction of multi-lamellar liposomes and no existence of higher order phases.

The long-term stability of the three types of lipid nanoparticles investigated here was confirmed using DLS and synchrotron SAXS; both the particle size and the internal lipid nano-structures were stable for at least two months stored at 4 °C (Table 1 and Figure S1). The morphology of the particles and their internal structure were also visualised by cryo-TEM (Figure S2). The finding that DSPE-$PEG_{Mw=3400}$ polymer stabilises self-assembled LCNPs presents the possibility of surface modification of LCNPs. One could take advantage of various functional groups such as maleimide, amine, biotin at the PEG chain end for bioconjugation on the LCNP surface.

2. *Anti-EGFR Fab' conjugation to LCNPs*

We prepared anti-EGFR Fab' with active thiol groups to conjugate with LCNPs functionalised by DSPE-PEG-mal. Figure S3A presents the SDS-PAGE gel results after conjugating Fab' to the cubosome surface at five different conjugation ratios, presented by the maleimide-to-thiol ratio. A negative control was performed by incubation of Fab' and nanoparticles stabilised by DSPE-PEG polymers without maleimide groups. The Fab' can be

identified at 55 kDa (Figure S3A). There was some TCEP-mediated reduction of the intermolecular disulfide bonds as seen from the presence of 26 and 28 kDa light chain (LC) and heavy chain (HC) bands under the non-reduced condition.

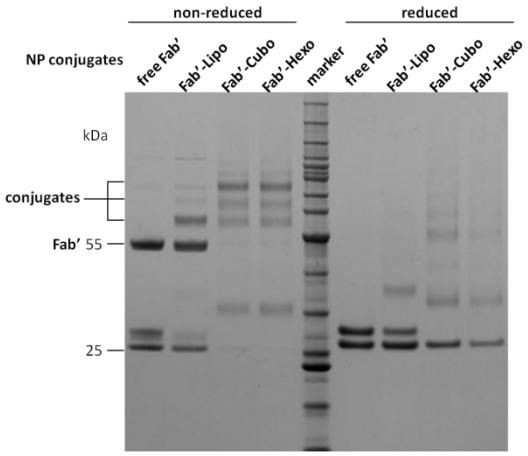

Figure 3: SDS-PAGE of conjugating anti-EGFR Fab' to liposomes, cubosomes and hexosomes at a maleimide-to-thiol ratio of 26:1. Fab' concentrations in all samples were kept constant for comparison.

When incubated with maleimide-functionalised cubosomes, each Fab' was able to react with 1, 2, or 3 molecules of DSPE-PEG-mal (Figure S3A, non-reduced lanes), indicated by three distinctive bands corresponding to the number of DSPE-PEG-mal molecules attached to Fab'. It could be seen that increasing the amount of maleimide groups in cubosomes resulted in more conjugation as indicated by the stronger appearance of the conjugated Fab' bands (Figure S3A, non-reduced lanes). Integrated image analysis of the gel showed that 95% of the Fab' was conjugated at the molar ratio of 26 maleimide groups per thiol group.

Under the reduced condition, HC and LC of Fab's were separated (Figure S3A, reduced lanes). The LC band (26 kDa) remained constant in mass whereas the HC band exhibited retarded migration, indicative of DSPE-PEG-mal reacting with the thiol groups

located in the HC hinge region of the Fab'. Conjugation of Fab's to maleimide-functionalised hexosomes exhibited similar conjugation efficiency and location as cubosomes (Figure S3B).

Figure 3 shows the comparison of the conjugation efficiency of the Fab' to liposomes, cubosomes and hexosomes. The SDS-PAGE data showed that conjugation of Fab' to cubosomes and hexosomes was significantly more efficient than that to liposomes, as there was negligible amount of free Fab' in the lanes of conjugated cubosomes and hexosomes under the non-reduced condition. In this particular case, integrated image analysis showed that conjugating Fab' to the surfaces of cubosomes and hexosomes reached 99% (Figure 3, Lanes Fab'-Cubo & Fab'-Hexo). This, however, was not the case for liposomes where only 20% of Fab' were conjugated (Figure 3, Lane Fab'-Lipo). The conjugation efficiency of Fab' to the maleimide-functionalised cubosomes and hexosomes in 5 replicates all recorded 95-99% but only around 20% for liposomes. This high conjugation efficiency may reduce the purification steps required for future *in vivo* use of these targeted nanoparticles. The DLS data of conjugated nanoparticles in Table 1 showed that the conjugation reaction did not significantly affect the size of the nanoparticles.

The low conjugation efficiency of Fab' to liposomes using maleimide-thiol reaction was consistent with previous studies.[20, 21] Mamot *et al.* used a post-insertion method to conjugate anti-EGFR Fab' of the C225 mAb to the surface of liposomes made of DSPC, cholesterol and DSPE-PEG. The post-insertion method involved conjugating Fab' to DSPE-PEG-mal micelles then incubating the conjugates with pre-formed liposomes at 55 °C.[20, 21] They reported that 30-50% of Fab' was conjugated to the micelles and then 75-85% of the conjugates inserted into pre-formed liposomes.[20, 21]

One reason for the low conjugation efficiency observed with liposomes could be that many functional maleimide groups orient toward the vesicle's lumen rather than the outer

surface. In cubosomes and hexosomes, Chong et al. examined the role of the PEG length of several triblock copolymers in maintaining colloidal stability of cubosomes and found that the limited internal water channel size of LCNPs restricts the internalisation of polymers with longer PEG chains restricting their adsorption to the particle surface.[72] Furthermore, in continuous lipid systems such as the hexagonal and cubic phases, DSPE-PEG-mal molecules can diffuse to the surface of the particle. Therefore, the maleimide groups may be more accessible (and in a greater surface concentration) on the surface of LCNPs for Fab' conjugation.

The cryo-TEM images of purified Fab'-conjugated cubosomes and hexosomes showed that the internal self-assembled cubic and hexagonal phases were retained after bioconjugation (Figure 4A & 4B). This result is consistent with the synchrotron SAXS analysis. Some co-existing small vesicles and cubosomes were observed. However, this is a typical phenomenon observed for the phytantriol system.[73] The cryo-TEM image of conjugated liposomes showed a monodisperse population of unilamellar vesicles in this particular field (Figure 4C). Additional cryo-TEM images of morphologies observed are presented in the Supplementary Information, Figure S2.

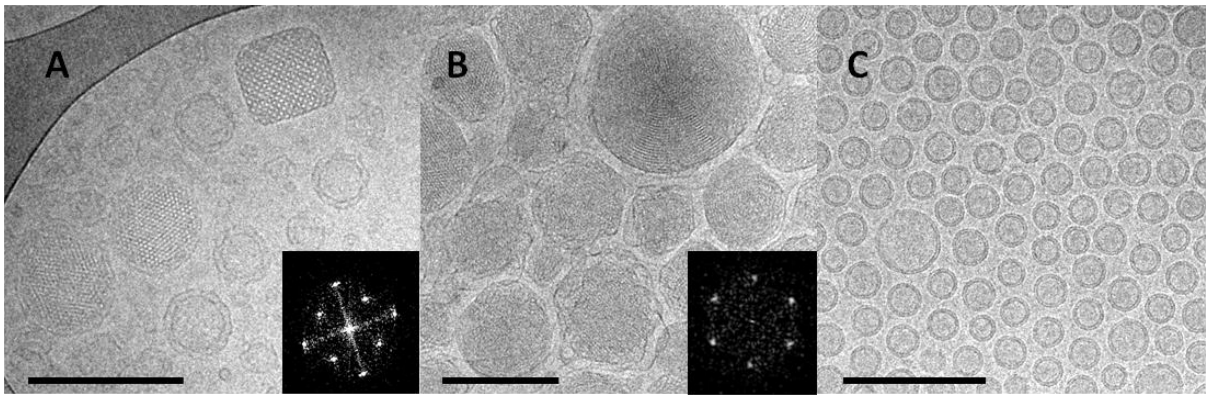

Figure 4: Representative cryo-TEM images of anti-EGFR Fab'-conjugated A) phytantriol cubosomes, B) phytantriol hexosomes, and C) unilamellar liposomes (DSPC:cholesterol). Fourier transforms of selected cubosomes and hexosomes are included to confirm the cubic and hexagonal structures, respectively. Scale bars represent 200 nm.

3. *Ligand binding activity of anti-EGFR Fab'-conjugated nanoparticles*

A key *in vitro* assessment for the development of actively targeted nanoparticles is to quantify the binding efficacy of the conjugated targeting moieties. The fusion protein of sEGFR501.Fc which has been shown to have high affinity for anti-EGFR ligands and contain epitopes recognised by the 528 mAb used in this study.[64-66] A competition ligand binding assay was performed to assess the binding efficacy of the anti-EGFR Fab' pre- and post-nanoparticle conjugation. The Fc region of sEGFR501.Fc was immobilised to a protein G-coated plate exposing the ligand binding site for the competition binding of Fab'-nanoparticles and Eu-EGF (Figure 5A). The binding assay showed that the Fab' from the 528 mAb and the corresponding conjugated nanoparticles had a high affinity for the immobilised EGFR501.Fc target in the IC50 range of $5\text{-}26\times10^{-9}$ M (Figure 5B). This result is comparable to the Fab'2 fragment of the 528 mAb and a human recombinant EGF (rHuEGF) (Figure S4). The 'bare' nanoparticles with no Fab' showed no inhibition of Eu-EGF binding to the target.

The IC50 values of the Fab' on the surface of liposomes (23 nM), cubosomes (24 nM) and hexosomes (26 nM) were higher than the free Fab' (5.6 nM). The slight decrease in the binding affinity of the conjugates could be due to steric hindrance at the particle surface by the PEGylated lipid layer. The extent of the change in affinity is comparable to findings by Rauscher et al. (2014), who have investigated the binding affinity of a bispecific antibody to hapten-conjugated liposomes using surface plasmon resonance (SPR).[74] It was found that when hapten was conjugated to the PEG end of DSPE-PEG polymers in liposomes, there was a 4-fold increase in the K_d value (6.3 nM) compared to soluble hapten binding to the antibody (1.4 nM). The study also found that when hapten was conjugated directly to DSPE on the liposome surface, the antibody binding affinity decreased with increased fraction of DSPE-PEG polymers in liposomes as well as increased PEG length. This decrease was attributed to

the fact that steric hindrance at the nanoparticle surface caused by PEGylation can slightly affect the binding affinity of the conjugated molecules.

In summary, anti-EGFR Fab' was successfully conjugated to phytantriol-based LCNPs functionalised by DSPE-$PEG_{Mw=3400}$-mal. The conjugation remained stable for at least two months at 4 °C due to the covalent coupling of thiol-maleimide reaction as demonstrated by SDS-PAGE (data not shown). Since the conjugation occurred to the hinge region of the Fab' HC to the maleimide group of the PEG polymer grafted on lipid nanoparticles (Figure 1C), the ligand binding site was oriented outward, exhibiting high affinity for the target.

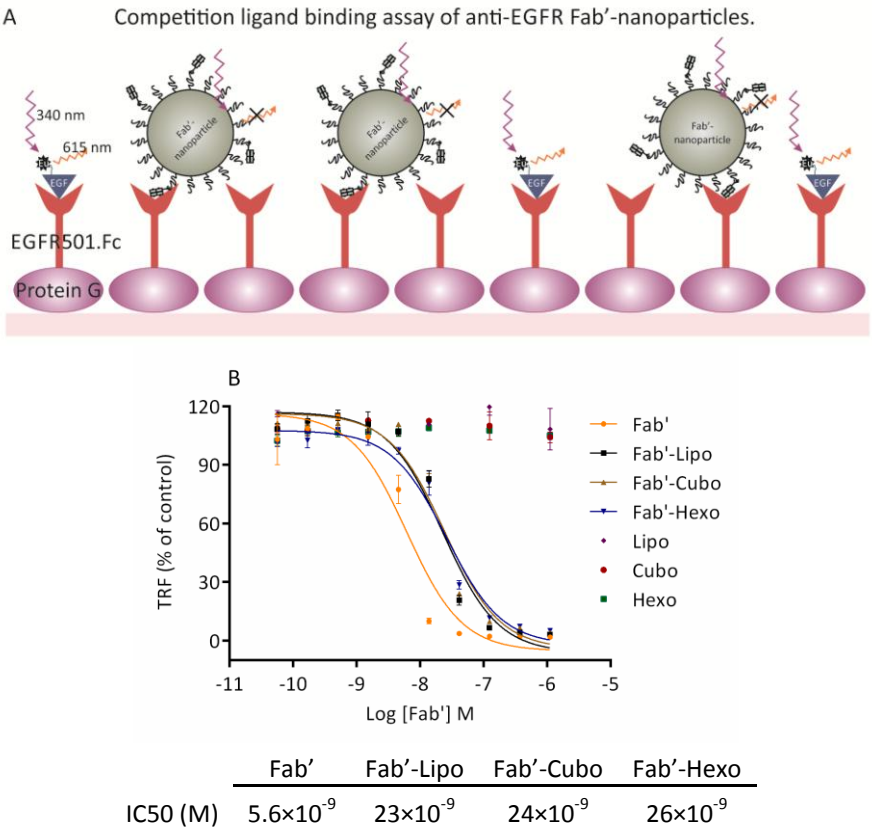

	Fab'	Fab'-Lipo	Fab'-Cubo	Fab'-Hexo
IC50 (M)	5.6×10^{-9}	23×10^{-9}	24×10^{-9}	26×10^{-9}

Figure 5: A) Schematic presentation of the competition ligand binding assay of anti-EGFR Fab'-nanoparticles. The Fab'-nanoparticles competed with Eu-EGF to bind to the immobilised EGFR target, sEGFR501.Fc. B) Ligand binding affinities of Fab'-nanoparticles. The competition assay was performed using Eu-EGF (100 pM) to dilute the Fab'-

nanoparticles at a range of Fab' concentrations as indicated. Values are normalised to the signal of Eu-EGF alone (100%) with each assay point representing the mean of triplicates.

Conclusion

Retaining targeting specificity and affinity following conjugation of mAb or Fab' to nanoparticles is key to ensure that the next generation of actively targeted nanoparticles can be fabricated. In this work, DSPE-PEG-mal with 70 PEG units was demonstrated to be a feasible polymer to stabilise phytantriol-based LCNPs exposing the functional maleimide groups on the surface. High conjugation efficiency was achieved by coupling anti-EGFR Fab' to LCNPs using the thiol-maleimide reaction. The conjugates retained high ligand binding affinities to the EGFR target and remained stable with respect to nanoparticle size and the internal lipid nanostructures. The fabrication of surface-active LCNPs presented here is not limited to thiol-maleimide chemistry and in principle could be applied to other bioconjugation experiments of interest to attach ligands to LCNPs. The active targeting of LCNPs shown here is a significant advance in the development of next generation nanomedicines. Future studies will combine the active targeting ability of LCNPs demonstrated here in with high therapeutic payload properties for targeted drug delivery in vitro and in vivo.

Acknowledgements

We sincerely thank Dr. Timothy E. Adams for his insightful discussion and the CSIRO OCE Science Team for the postdoctoral project funding. This research was undertaken, in part, on the SAXS/WAXS beamline at the Australian Synchrotron, Victoria, Australia.

Notes and References

Electronic Supplementary Information (ESI) available: Figure S1-S4

1. S.-E. Jin, H.-E. Jin and S.-S. Hong, *BioMed Res. Int.*, 2014, **2014**, Article ID 814208, doi:10.1155/2014/814208.
2. Y. Namiki, T. Fuchigami, N. Tada, R. Kawamura, S. Matsunuma, Y. Kitamoto and M. Nakagawa, *Acc. Chem. Res.*, 2011, **44**, 1080.
3. S. Nazir, T. Hussain, A. Ayub, U. Rashid and A. J. MacRobert, *Nanomed. Nanotechnol.*, 2014, **10**, 19.
4. A. Z. Wang, R. Langer and O. C. Farokhzad, *Annu. Rev. Med.*, 2012, **63**, 185.
5. Y. Li, J. Wang, M. G. Wientjes and J. L. Au, *Adv. Drug Deliv. Rev.*, 2012, **64**, 29.
6. R. Solaro, F. Chiellini and A. Battisti, *Materials*, 2010, **3**, 1928.
7. J. D. Byrne, T. Betancourt and L. Brannon-Peppas, *Adv. Drug Deliv. Rev.*, 2008, **60**, 1615.
8. J. M. Montenegro, V. Grazu, A. Sukhanova, S. Agarwal, J. M. de la Fuente, I. Nabiev, A. Greiner and W. J. Parak, *Adv. Drug Deliv. Rev.*, 2013, **65**, 677.
9. C. R. Chong and P. A. Janne, *Nat. Med.*, 2013, **19**, 1389.
10. T. Sasaki, K. Hiroki and Y. Yamashita, *Biomed. Res. Int.*, 2013, **2013**, 546318.
11. T. P. Garrett, A. W. Burgess, H. K. Gan, R. B. Luwor, G. Cartwright, F. Walker, S. G. Orchard, A. H. Clayton, E. C. Nice, J. Rothacker, B. Catimel, W. K. Cavenee, L. J. Old, E. Stockert, G. Ritter, T. E. Adams, P. A. Hoyne, D. Wittrup, G. Chao, J. R.

Cochran, C. Luo, M. Lou, T. Huyton, Y. Xu, W. D. Fairlie, S. Yao, A. M. Scott and T. G. Johns, *Proc. Natl. Acad. Sci. USA*, 2009, **106**, 5082.

12. C. A. Gerdes, V. G. Nicolini, S. Herter, E. van Puijenbroek, S. Lang, M. Roemmele, E. Moessner, O. Freytag, T. Friess, C. H. Ries, B. Bossenmaier, H. J. Mueller and P. Umana, *Clin. Cancer Res.*, 2013, **19**, 1126.
13. K. Shigeta, T. Hayashida, Y. Hoshino, K. Okabayashi, T. Endo, Y. Ishii, H. Hasegawa and Y. Kitagawa, *PloS One*, 2013, **8**, e66302.
14. D. B. Kirpotin, D. C. Drummond, Y. Shao, M. R. Shalaby, K. Hong, U. B. Nielsen, J. D. Marks, C. C. Benz and J. W. Park, *Cancer Res.*, 2006, **66**, 6732.
15. H. Matsudaira, T. Asakura, K. Aoki, Y. Searashi, T. Matsuura, H. Nakajima, H. Tajiri and K. Ohkawa, *Int. J. Oncol.*, 2010, **36**, 77.
16. S. C. Owen, N. Patel, J. Logie, G. Pan, H. Persson, J. Moffat, S. S. Sidhu and M. S. Shoichet, *J. Control Release*, 2013, **172,** 395.
17. Y. Yuan, S. Chen, T. Paunesku, S. C. Gleber, W. C. Liu, C. B. Doty, R. Mak, J. Deng, Q. Jin, B. Lai, K. Brister, C. Flachenecker, C. Jacobsen, S. Vogt and G. E. Woloschak, *ACS Nano*, 2013, **7,** 10502.
18. J. Lehtinen, M. Raki, K. A. Bergström, P. Uutela, K. Lehtinen, A. Hiltunen, J. Pikkarainen, H. Liang, S. Pitkänen, A.-M. Määttä, R. A. Ketola, M. Yliperttula, T. Wirth and A. Urtti, *PloS One*, 2012, **7**, e41410.
19. A. N. Lukyanov, T. A. Elbayoumi, A. R. Chakilam and V. P. Torchilin, *J. Control Release*, 2004, **100**, 135.
20. C. Mamot, D. C. Drummond, U. Greiser, K. Hong, D. B. Kirpotin, J. D. Marks and J. W. Park, *Cancer Res.*, 2003, **63**, 3154.
21. C. Mamot, D. C. Drummond, C. O. Noble, V. Kallab, Z. Guo, K. Hong, D. B. Kirpotin and J. W. Park, *Cancer Res.*, 2005, **65**, 11631.

22. D. Kirpotin, J. W. Park, K. Hong, S. Zalipsky, W. L. Li, P. Carter, C. C. Benz and D. Papahadjopoulos, *Biochemistry*, 1997, **36**, 66.

23. J. W. Park, K. Hong, D. B. Kirpotin, G. Colbern, R. Shalaby, J. Baselga, Y. Shao, U. B. Nielsen, J. D. Marks, D. Moore, D. Papahadjopoulos and C. C. Benz, *Clin. Cancer Res.*, 2002, **8**, 1172.

24. S. Hussain, A. Plückthun, T. M. Allen and U. Zangemeister-Wittke, *Mol. Cancer Ther.*, 2006, **5**, 3170.

25. R. Wang, R. Xiao, Z. Zeng, L. Xu and J. Wang, *Int. J. Nanomed.*, 2012, **7**, 4185.

26. T. Yang, M. K. Choi, F. D. Cui, J. S. Kim, S. J. Chung, C. K. Shim and D. D. Kim, *J. Control Release*, 2007, **120**, 169.

27. J. V. Jokerst, T. Lobovkina, R. N. Zare and S. S. Gambhir, *Nanomedicine (Lond)*, 2011, **6**, 715.

28. M. V. Pasquetto, L. Vecchia, D. Covini, R. Digilio and C. Scotti, *J. Immuno.*,2011, **34**, 611.

29. D. Vllasaliu, R. Fowler and S. Stolnik, *Expert Opin. Drug Deliv.*, 2014, **11**, 139.

30. B. Angelov, A. Angelova, S. K. Filippov, M. Drechsler, P. Štěpánek and S. Lesieur, *ACS Nano*, 2014, **8**, 5216.

31. A. Angelova, B. Angelov, M. Drechsler and S. Lesieur, *Drug Discovery Today*, 2013, **18**, 1263.

32. A. Angelova, B. Angelov, R. Mutafchieva, S. Lesieur and P. Couvreur, *Acc. Chem. Res.*, 2010, **44**, 147.

33. C. E. Conn and C. J. Drummond, *Soft Matter*, 2013, **9**, 3449.

34. W. K. Fong, T. Hanley and B. J. Boyd, *J. Control Release*, 2009, **135**, 218.

35. C. Géral, A. Angelova and S. Lesieur, *Pharmaceutics*, 2013, **5**, 127.

36. V. Jain, N. K. Swarnakar, P. R. Mishra, A. Verma, A. Kaul, A. K. Mishra and N. K. Jain, *Biomaterials*, 2012, **33**, 7206.

37. X. Mulet, B. J. Boyd and C. J. Drummond, *J.Colloid Interface Sci.*, 2013, **393**, 1.

38. X. Mulet, D. F. Kennedy, C. E. Conn, A. Hawley and C. J. Drummond, *Int. J. Pharm.*, 2010, **395**, 290.

39. S. Murgia, S. Bonacchi, A. M. Falchi, S. Lampis, V. Lippolis, V. Meli, M. Monduzzi, L. Prodi, J. Schmidt, Y. Talmon and C. Caltagirone, *Langmuir*, 2013, **29**, 6673.

40. T.-H. Nguyen, T. Hanley, C. J. H. Porter, I. Larson and B. J. Boyd, *J. Pharm. Pharmacol.*, 2010, **62**, 856.

41. T.-H. Nguyen, T. Hanley, C. J. H. Porter, I. Larson and B. J. Boyd, *J. Pharm. Pharmacol.*, 2010, **62**, 844.

42. S. B. Rizwan, W. T. McBurney, K. Young, T. Hanley, B. J. Boyd, T. Rades and S. Hook, *J. Control Release*, 2013, **165**, 16.

43. S. M. Sagnella, X. Gong, M. J. Moghaddam, C. E. Conn, K. Kimpton, L. J. Waddington, I. Krodkiewska and C. J. Drummond, *Nanoscale*, 2011, **3**, 919.

44. N. K. Swarnakar, K. Thanki and S. Jain, *Pharma. Res.*, 2014, **31,** 1219.

45. Z. W. Yang, M. W. Chen, M. H. Yang, J. Chen, W. J. Fang and P. Xu, *Int. J. Nanomed.*, 2014, **9**, 327.

46. G. Zhen, T. M. Hinton, B. W. Muir, S. Shi, M. Tizard, K. M. McLean, P. G. Hartley and P. Gunatillake, *Mol. Pharm.*, 2012, **9**, 2450.

47. C. Fong, T. Le and C. J. Drummond, *Chem. Soc. Rev.*, 2012, **41**, 1297.

48. B. Angelov, A. Angelova, B. Papahadjopoulos-Sternberg, S. V. Hoffmann, V. Nicolas and S. Lesieur, *J. Phys. Chem. B*, 2012, **116**, 7676.

49. A. Angelova, M. Ollivon, A. Campitelli and C. Bourgaux, *Langmuir*, 2003, **19**, 6928.

50. A. Angelova, B. Angelov, M. Drechsler, V. M. Garamus and S. Lesieur, *Int. J. Pharm.*, 2013, **454,** 625.

51. S. J. Fraser, R. M. Dawson, L. J. Waddington, B. W. Muir, X. Mulet, P. G. Hartley, F. Separovic and A. Polyzos, *Australian J. Chem.*, 2011, **64**, 46.

52. H.-H. Shen, V. Lake, A. P. Le Brun, M. James, A. P. Duff, Y. Peng, K. M. McLean and P. G. Hartley, *Biomaterials*, 2013, **34**, 8361.

53. H. Wu, J. Li, Q. Zhang, X. Yan, L. Guo, X. Gao, M. Qiu, X. Jiang, R. Lai and H. Chen, *Eur. J. Pharm. Biopharm.*, 2012, **80**, 368.

54. J. Zhai, L. Waddington, T. J. Wooster, M. I. Aguilar and B. J. Boyd, *Langmuir*, 2011, **27**, 14757.

55. J. Y. T. Chong, X. Mulet, L. J. Waddington, B. J. Boyd and C. J. Drummond, *Langmuir*, 2012, **28**, 9223.

56. J. Barauskas and T. Landh, *Langmuir*, 2003, **19**, 9562.

57. Y.-D. Dong, A. W. Dong, I. Larson, M. Rappolt, H. Amenitsch, T. Hanley and B. J. Boyd, *Langmuir*, 2008, **24**, 6998.

58. S. J. Fraser, X. Mulet, A. Hawley, F. Separovic and A. Polyzos, *J. Colloid Interface Sci.*, 2013, **408,** 117.

59. G. L. Ellman, *Arch. Biochem. Biophys.*, 1959, **82**, 70.

60. C. Riener, G. Kada and H. Gruber, *Anal. Bioanal. Chem.*, 2002, **373**, 266.

61. W. S. Rasband, ImageJ, U.S. National Institutes of Health, Bethesda, Maryland, USA, 1997-2014.

62. X. Mulet, C. E. Conn, C. Fong, D. F. Kennedy, M. J. Moghaddam and C. J. Drummond, *Acc. Chem. Res.*, 2013, **46**, 1497.

63. J. M. Seddon, A. M. Squires, C. E. Conn, O. Ces, A. J. Heron, X. Mulet, G. C. Shearman and R. H. Templer, *Philos. Trans. Series A, Math., Phys. Eng. Sci.*, 2006, **364**, 2635.

64. T. E. Adams, E. J. Koziolek, P. H. Hoyne, J. D. Bentley, L. Lu, G. Lovrecz, C. W. Ward, F. T. Lee, A. M. Scott, A. D. Nash, J. Rothacker, E. C. Nice, A. W. Burgess and T. G. Johns, *Growth Factors*, 2009, **27**, 141.

65. T. C. Elleman, T. Domagala, N. M. McKern, M. Nerrie, B. Lönnqvist, T. E. Adams, J. Lewis, G. O. Lovrecz, P. A. Hoyne, K. M. Richards, G. J. Howlett, J. Rothacker, R. N. Jorissen, M. Lou, T. P. J. Garrett, A. W. Burgess, E. C. Nice and C. W. Ward, *Biochemistry*, 2001, **40**, 8930.

66. M. P. Madej, G. Coia, C. C. Williams, J. M. Caine, L. A. Pearce, R. Attwood, N. A. Bartone, O. Dolezal, R. M. Nisbet, S. D. Nuttall and T. E. Adams, *Biotechnol. Bioeng.*, 2012, **109**, 1461.

67. C. Nilsson, J. Østergaard, S. W. Larsen, C. Larsen, A. Urtti and A. Yaghmur, *Langmuir*, 2014, **30**, 6398.

68. C. Bonechi, S. Martini, L. Ciani, S. Lamponi, H. Rebmann, C. Rossi and S. Ristori, *PloS One*, 2012, **7**, e41438.

69. N. Kučerka, Y. Liu, N. Chu, H. I. Petrache, S. Tristram-Nagle and J. F. Nagle, *Biophys. J.*, 2005, **88**, 2626.

70. J. A. Bouwstra, G. S. Gooris, W. Bras and H. Talsma, *Chem. Phys. Lipids*, 1993, **64**, 83.

71. S. Ristori, J. Oberdisse, I. Grillo, A. Donati and O. Spalla, *Biophys. J.*, 2005, **88**, 535.

72. J. Y. T. Chong, X. Mulet, L. J. Waddington, B. J. Boyd and C. J. Drummond, *Soft Matter*, 2011, **7**, 4768.

73. Y.-D. Dong, I. Larson, T. J. Barnes, C. A. Prestidge and B. J. Boyd, *ACS Appl. Mater. Interfaces*, 2011, **3**, 1771.

74. A. Rauscher, M. Frindel, C. Maurel, M. Maillasson, P. Le Saëc, H. Rajerison, J. F. Gestin, J. Barbet, A. Faivre-Chauvet and M. Mougin-Degraef, *Nucl. Med. Biol.*, 2014, **41, Supplement**, e66.